Perturbative studies of the conductivity in the vortex-liquid regime

T. Blum*† and M. A. Moore*
*Department of Physics, University of Manchester, Manchester, M13 9PL, United Kingdom.
†Department of Physics, Jesse W. Beams Laboratory, McCormick Rd., University of Virginia, Charlottesville, VA 22901.
(February 1, 2008)

We calculate the Aslamazov-Larkin term of the conductivity in the presence of a magnetic field applied along the c axis from the time-dependent Ginzburg-Landau equation perturbatively using two approaches. In the first a uniform electric field is explicitly applied; in the second the Kubo formula is used to extract the linear response. The former yields a version of the flux-flow formula for the uniform ab-plane conductivity, $\sigma_{xx}(\mathbf{k}=\mathbf{0})$, that holds to all orders of perturbation theory. Obtaining the same result from the Kubo formula requires considerable cancellation of terms. We also use the Kubo calculation to examine the nonlocal ab-plane conductivity, $\sigma_{xx}(\mathbf{k}\neq\mathbf{0})$ (where the cancellations no longer occur), as well as the nonlocal c-axis conductivity $\sigma_{zz}(\mathbf{k}\neq\mathbf{0})$, and look for the perturbative precursors of the growing viscous length scales. In addition, we consider the effects of weak disorder — both uncorrelated (point defects) and correlated (columnar and planar defects).

I. INTRODUCTION

Recent experiments on $YBCO$ have exploited nonuniform current distributions to reveal the nonlocal nature of the conductivity in the vortex-liquid regime. The conductivity is nonlocal if the current at a site $\mathbf{r}$ is determined not only by $\mathbf{E}(\mathbf{r})$ the electric field at $\mathbf{r}$ but also by the fields at other sites $\mathbf{E}(\mathbf{r}')$. The conductivity is always nonlocal on some microscopic scale, but the term "nonlocal" is generally reserved for cases in which the length scale involved is much longer than some underlying microscopic one. A nonlocal conductivity implies a nonlocal resistivity, though the length scales on which each varies may differ. Nonlocality may result if the "integrity" of the vortex along the c axis is maintained (*i.e.* not much cutting and reconnecting) as then a current applied at the top of a sample will yield a response not only at the top but also at the bottom. The interactions between vortices may also lead to nonlocal effects within the ab plane.

The nonlocal nature of the conductivity has been studied by Safar *et al.*[1] They injected small currents into the top of a sample with a magnetic field applied along the z axis. They extracted the current in one case from a second contact along the top and in another case from the bottom. In each configuration a series of voltage differences were taken. The results were then analyzed assuming a local though anisotropic conductivity ($\sigma_{xx}\neq\sigma_{zz}$) — the so-called modified Montgomery analysis. Safar *et al.*[1] found an effective value for the ratio σ_{xx}/σ_{zz} for each configuration and discovered a discrepancy of order $\sim 10^5$ between them. The inadequacy of the local analysis is taken as evidence for a nonlocal conductivity. Similar evidence for nonlocal effects in BSCCO has been reported[2].

It should be pointed out that the nonlocal interpretation has been questioned both on theoretical[3] and experimental[4] grounds. It should also be noted that the large effects seen by Safar *et al.*[1] were in heavily twinned samples. Evidence for nonlocal effects in pure samples is somewhat weaker. López *et al.*[5] made a direct comparison of twinned and untwinned samples. In the first of the current configurations described above (current into and out of the top), they took voltage measurements across the top and bottom of their samples as a function of temperature. In twinned samples of YBCO, the resulting curves V_{top} and V_{bot} became almost indistinguishable at temperatures above the melting transition, indicative of a long c-axis length scale in the vortex liquid regime. In untwinned crystals, on the other hand, the curves only met at the melting transition. This result demonstrates the enhancement of the vortex-line integrity and hence nonlocality by the correlated defect.

On the theoretical side nonlocal conductivity has been studied within the hydrodynamic framework[6]. We are assuming a linear but nonlocal relationship between current and electric field, *i.e.* an integral version of Ohm's law

$$j_\mu(\mathbf{r}) = \int \sigma_{\mu\nu}(\mathbf{r},\mathbf{r}')E_\nu(\mathbf{r}')d\mathbf{r}', \tag{1}$$

where $\sigma_{\mu\nu}(\mathbf{r},\mathbf{r}') \neq \sigma_{\mu\nu}\delta(\mathbf{r}-\mathbf{r}')$. If the system is translationally invariant, Fourier transforming equation (1) results in

$$j_\mu(\mathbf{k}) = \sigma_{\mu\nu}(\mathbf{k})\ E_\nu(\mathbf{k}), \tag{2}$$

where nonlocality now implies $\sigma_{\mu\nu}(\mathbf{k}) \neq$ const. The emphasis is on the large-distance behavior in real space and so presumably on the small-$\mathbf{k}$ behavior of the Fourier transform. Huse and Majumdar[7] explored a hydrodynamic approach, in which the small-$\mathbf{k}$ expansion of $\sigma_{\mu\nu}(\mathbf{k})$ is truncated as follows:

$$\sigma_{\mu\nu}(\mathbf{k}) \ = \ \sigma_{\mu\nu}(\mathbf{0}) \ + \ \mathbf{S}_{\mu\alpha\beta\nu}\ \mathbf{k}_\alpha\mathbf{k}_\beta. \tag{3}$$

In the example they work out in detail to explain features seen by Safar *et al.*, they include only one S: S_{xzzx}. It models the "tilt viscosity" — which measures the influence of pancake vortices moving in one ab plane on those moving in another when they travel with different velocities.[7]

Stability requires that $\sigma_{\mu\nu}(\mathbf{k})$ be a positive definite matrix. For the hydrodynamic form of $\sigma_{\mu\nu}(\mathbf{k})$, it implies, for example, that S_{xzzx} and S_{xxxx} must be positive. When these conditions are met, one finds that the *resistivity* decays with a length scale of order $(\sqrt{S/\sigma})$, which is in turn the length scale of the electric-field and current distributions.[7] (The hydrodynamic approach also predicts surface currents which supposedly should be spread out over some small length scale not accessible by that technique.) Recent calculations[8,9] starting from the time-dependent Ginzburg-Landau (TDGL) equation find that many of the S's do not have the requisite sign — at least not for clean samples at high temperatures. Those calculations were taken only to Gaussian order (lowest order in perturbation theory); the purpose of the present paper is to go beyond Gaussian order and also to explore the effect of various sorts of defects: point, columnar and planar. Recent simulations of the TDGL equations in two dimensions did find a region above the melting transition in which $S_{xxxx} \geq 0$.[10] (The problem of calculating the voltage distribution whether or not the conductivities are of the "hydrodynamic" form will be presented elsewhere.[11])

The first order of business is to calculate the uniform conductivity $\sigma_{\mu\nu}(\mathbf{0})$. The resistivity of clean samples of YBCO in the vortex-liquid regime varies smoothly with temperature until it experiences a sudden drop generally associated with the first-order melting transition to a pinned vortex solid. The temperature and field dependences in this smooth region agree with the flux-flow formula[12] which was originally conceived of in the vortex-solid phase where one pictures the translation of the entire unpinned vortex lattice. So how is it that the same physics applies in the vortex-liquid regime? The important feature of the flux-flow formula besides the absence of pinning by defects would seem to be its insensitivity to viscous effects. As it is the entire vortex system that moves, the amount of entanglement along the c-axis or the extent of crystalline order in the ab plane is irrelevant. It takes a nonuniform current distribution to probe such viscous effects.

We will determine $\sigma_{\mu\nu}(\mathbf{0})$ in two ways. First, we will consider the TDGL equation with an explicit uniform electric field applied, calculating the current and extracting $\sigma_{\mu\nu}(\mathbf{0})$ directly. Second, we will calculate the conductivity from the Kubo formula, a version of the fluctuation-dissipation theorem which yields the linear response of a system not too far from equilibrium. The electric field does not explicitly appear in the latter. We will see that a delicate cancellation of terms arising in the Kubo calculation is necessary for the two approaches to agree, and we will demonstrate this cancellation to second order in perturbation theory for the conductivity of two-dimensional samples. We will then proceed to examine the nonlocal effects within the Kubo formalism, see how the $\mathbf{k}=\mathbf{0}$ cancellation breaks down at $\mathbf{k}\neq\mathbf{0}$ and show how viscous effects may enter.

Next we consider the effect of disorder — first on the uniform conductivity. It would seem to have two competing effects. On one hand, defects pin the vortices and thus might lower the resistivity. On the other hand, they disrupt the formation of a vortex lattice[13] which is more readily pinned than individual vortices, and thus they might raise the resistivity. In fact, both effects are seen in the experiments of Fendrich *et al.*[14] in which point defects were induced by electron irradiation. Introducing the defects eliminated the sudden drop in resistivity at T_c. At temperatures above T_c, the irradiated sample had a lower resistivity; while at temperatures below T_c, it had a higher resistivity. Another outcome of inducing the defects is that the temperature and field dependence is no longer of the flux-flow type. At low temperatures an activated form might be expected[15], but such considerations are beyond the scope of the present work which employs standard perturbation theory. We will examine the effect of these defects in the weak disorder limit.

Even the lowest-order calculation of $\sigma_{\mu\nu}(\mathbf{k},\omega)$, the wave-vector and frequency-dependent conductivity, is cumbersome.[8,9] To simplify the results we will concentrate on the leading behavior. In the presence of a magnetic field, Landau levels provide a natural basis for calculating and describing various phenomena. Two energy scales naturally arise: the first is α_H, the energy of states in the $n=0$ or lowest Landau level (LLL); the second is the energy spacing between Landau levels given by $\hbar\omega_0$ with ω_0 the cyclotron frequency. We will gain an immense simplification by focusing on the regime in which $\alpha_H \ll \hbar\omega_0$, the so-called LLL approximation. Arguments based on the *renormalized* values of α_H and $\hbar\omega_0$ suggest that such a separation of scales holds over a significant portion of the vortex-liquid regime.[16] Note that $\alpha_H \ll \hbar\omega_0$ limit does not imply that only $n=0$ states are employed in a

calculation, although it usually does imply that the number of $n \neq 0$ states is kept to a minimum. Considering only fluctuations in the LLL states serves not only to simplify the calculations but also to regularize them.

Before presenting the calculations in detail let us highlight a couple key features. The Kubo formula for the conductivity involves the product of two current densities, and each current density involves a product of a Ψ and a Ψ^*, where Ψ is the superconducting order parameter. (See eqs. (34) and (35) below.) Thus, calculated in this way the conductivity is a "four-point" object, that is, it involves four Ψ fields. If these Ψ's are expanded in the Landau-level basis, a crucial question arises: how many of these four Ψ's can be in the LLL? Already we find a notable distinction between the c-axis conductivity, $\sigma_{zz}(\mathbf{0})$, for which the answer is all four and the ab-plane conductivity, $\sigma_{xx}(\mathbf{0})$, for which the answer is only two. As a result, in the LLL regime the characteristic time scale inherent in σ_{zz} is much larger than that in σ_{xx}. Another outcome is that in terms of LLL states ($\sigma_{xx}(\mathbf{0})$) is a two-point quantity and as such is independent of viscous effects which are related to four-point quantities.

Understanding the effect of random pinning in the vortex-liquid regime is no trivial matter.[17] When point disorder is added, translational invariance is destroyed. Moreover, while the division of $\sigma_{xx}(\mathbf{0})$ into $n = 0$ and $n \geq 1$ parts persists, the $n = 0$ component now becomes a four-point object sensitive to viscous effects. As a result the associated time and length scales may grow. The separation of $n = 0$ and $n \geq 1$ states also plays a role in the distinction between c-axis length scales in materials with correlated and uncorrelated disorder. To each energy level there is associated a c-axis length scale, and the one linked to the $n = 0$ level is much longer. It turns out that the c-axis length scale of σ_{xx} is controlled by the $n = 0$ states in the presence of columnar and planar defects but by the $n \geq 1$ states in the presence of point defects.

The rest of the paper is organized as follows. In the next section we lay the groundwork for the calculations that follow by constructing the Green's function and correlation function from the TDGL equation. In the section following that we calculate the uniform conductivity, $\sigma_{xx}(\mathbf{0})$, first by explicitly applying the electric field and then via the Kubo formula. We then move on to consider the nonlocal conductivity $\sigma_{xx}(\mathbf{k})$. After that we examine the conductivity of films. We then consider the effect of weak disorder and finally summarize.

II. TIME-DEPENDENT GINZBURG-LANDAU THEORY

We begin with the usual Ginzburg-Landau free-energy functional $\mathcal{F}[\Psi]$ for the superconducting order parameter $\Psi(\mathbf{r}, t)$ in a magnetic field

$$\mathcal{F}[\Psi] = \int d^3\mathbf{r} \left[\sum_{j=x,y,z} \frac{|P_j \Psi|^2}{2m_j} + \alpha |\Psi|^2 + \frac{\beta}{2} |\Psi|^4 + \frac{1}{2\mu_0} (\nabla \times \mathbf{A})^2 \right]. \tag{4}$$

where $\mathbf{A}$ is the vector potential and P_j is the j^{th} component of the momentum operator given by

$$P_j = \frac{\hbar}{i} \frac{\partial}{\partial r_j} - e^* A_j(\mathbf{r}) \tag{5}$$

with $e^* = 2e$. This combination arises for reasons of gauge invariance. We allow for two masses $m_{x,y} = m_{ab}$ and $m_z = m_c$ to reflect to some extent the anisotropy of high T_c materials; of course, the calculations can be extended to the Lawrence-Doniach model in which the layering is treated more explicitly.

Next, we choose a simple relaxational dynamics for Ψ given by the time-dependent Ginzburg-Landau equation

$$\frac{1}{\Gamma} \left(\frac{\partial}{\partial t} + \frac{i e^* \Phi(\mathbf{r}, t)}{\hbar} \right) \Psi(\mathbf{r}, t) = -\frac{\delta \mathcal{F}[\Psi]}{\delta \Psi^*(\mathbf{r}, t)} + \eta(\mathbf{r}, t). \tag{6}$$

The field $\Phi(\mathbf{r}, t)$ is related to the chemical potential which accompanies the time derivative in order to maintain gauge invariance; in what follows we will use the approximation that $\Phi(\mathbf{r}, t)$ is the scalar electric potential.[18–20] The thermal fluctuations are represented by the noise $\eta(\mathbf{r}, t)$, which has zero average and δ-function correlations

$$\langle \eta^*(\mathbf{r}, t)\ \eta(\mathbf{r}', t') \rangle = \frac{2 k_B T}{\Gamma}\ \delta(\mathbf{r} - \mathbf{r}')\ \delta(t - t'). \tag{7}$$

The noise strength is chosen so that in the absence of a driving electric field, the distribution of Ψ's, $\mathcal{P}[\Psi]$, evolves toward its equilibrium solution

$$\mathcal{P}[\Psi] \propto \exp \left\{ -\frac{1}{k_B T} \int d^3\mathbf{r}\ \mathcal{F}[\Psi] \right\}. \tag{8}$$

We take Γ, the kinetic coefficient, to be real. Note that a complex kinetic coefficient ($\Gamma^{-1} \to \Gamma_0^{-1} + i\lambda_0^{-1}$ in eq. (6) but $\Gamma^{-1} \to \Gamma_0^{-1}$ in eq. (7)) is required to model the Hall conductivity σ_{xy}.[20,21]

The TDGL equation is supplemented by

$$\nabla \times \nabla \times \mathbf{A} = \mu_0 \left[\mathbf{J^{(n)}} + \mathbf{J^{(s)}} \right], \tag{9}$$

where $\mathbf{J^{(n)}}$ is the normal current given by

$$\mathbf{J^{(n)}} = \sigma^{(n)} \left[-\nabla\Phi - \frac{\partial \mathbf{A}}{\partial t} \right] \tag{10}$$

and $\mathbf{J^{(s)}}$ is the superconducting current given by

$$J_j^{(s)}(\mathbf{r},t) = \frac{e^*}{2m_j} \left[P_{1j} + P_{2j}^* \right] \Psi^*(\mathbf{r_2},t)\Psi(\mathbf{r_1},t) \Big|_{\mathbf{r_1}=\mathbf{r_2}=\mathbf{r}}, \tag{11}$$

with P_j is the momentum operator (5). Eq. (9) is simply Maxwell's equation *sans* the Maxwell displacement current which is presumed negligibly small. Actually in this paper we concentrate solely on the TDGL equation, so that certain effects that enter with the Maxwell equations, such as backflow[22–24], will be missing.

Let us consider an electric field applied along the x direction: $\Phi(\mathbf{r},t) = -E\,x$ and a magnetic field applied in the z direction: ($\mathbf{A} = Bx\hat{y}$). The TDGL equation then becomes

$$\left[\frac{1}{\Gamma}\frac{\partial}{\partial t} + \mathcal{H}(\mathbf{r}) \right] \psi(\mathbf{r},t) = \eta(\mathbf{r},t) - \beta|\psi(\mathbf{r},t)|^2\psi(\mathbf{r},t), \tag{12}$$

where $\mathcal{H}$ is

$$\mathcal{H} = -\frac{\hbar^2}{2m_{ab}} \left(\frac{\partial^2}{\partial x^2} + \left(\frac{\partial}{\partial y} - \frac{ie^*Bx}{\hbar} \right)^2 \right) - \frac{\hbar^2}{2m_c}\frac{\partial^2}{\partial z^2} + \alpha - \frac{ie^*Ex}{\Gamma\hbar}. \tag{13}$$

For the calculations that follow we will need the Green's function which satisfies:

$$\left[\frac{1}{\Gamma}\frac{\partial}{\partial t} + \mathcal{H}(\mathbf{r}) \right] \; G(\mathbf{r},t;\mathbf{r}',t') \;=\; \delta(\mathbf{r}-\mathbf{r}')\;\delta(t-t'). \tag{14}$$

The Green's function serves as the inverse of the operator $(\Gamma^{-1}\partial_t + \mathcal{H})$, allowing us to rewrite the TDGL equation as

$$\Psi(\mathbf{r},t) = \int d\mathbf{r}' \int dt'\; G(\mathbf{r},t;\mathbf{r}',t') \left[\eta(\mathbf{r}',t') - \beta|\Psi(\mathbf{r}',t')|^2\Psi(\mathbf{r}',t') \right], \tag{15}$$

which we can write in a more symbolic form

$$\Psi_1 = G_{1,2}\eta_2 - \beta G_{1,2}\Psi_2^*\Psi_2\Psi_2. \tag{16}$$

and solve — at least formally — by iteration

$$\Psi_1 = G_{1,2}\eta_2 - \beta G_{1,2}G_{2,3}^*G_{2,4}G_{2,5}\eta_3^*\eta_4\eta_5 + O(\beta^2). \tag{17}$$

This expansion forms the basis for the standard perturbation theory in β.

We can construct $G(\mathbf{r},t;\mathbf{r}',t')$ from the eigenstates $\phi_n(k_y,k_z;\mathbf{r})$ and eigenvalues $E_n(k_y,k_z)$ of $\mathcal{H}$, which are

$$\phi_n(k_y,k_z;\mathbf{r}) = e^{ik_y y + ik_z z}\; u_n\left(\frac{x}{\ell} - k_y\ell - \frac{ivm_{ab}\ell}{\hbar^2\Gamma} \right), \tag{18}$$

and

$$E_n(k_y,k_z) = \frac{\hbar^2k_z^2}{2m_c} + \underbrace{\alpha + \frac{\hbar\omega_0}{2} + \frac{m_{ab}v^2}{2\hbar^2\Gamma^2}}_{\alpha_{EH}} + n\;\hbar\omega_0 - \frac{ik_yv}{\Gamma}, \tag{19}$$

where

$$\ell = \left(\frac{\hbar}{e^* B}\right)^{1/2}, \quad \omega_0 = \frac{e^* B}{m_{ab}} \quad \text{and} \quad v = \frac{E}{B}. \tag{20}$$

(ℓ is the magnetic length and is associated with the distance between vortices; ω_0 is the cyclotron frequency; and v is roughly speaking the speed at which the flux lines move.) The functions $u_n(s)$ are given by

$$u_n(s) = \frac{H_n(s)\, \exp\{-s^2/2\}}{\left(\ell\sqrt{\pi} 2^n n!\right)^{1/2}}, \tag{21}$$

where $H_n(s)$ are the Hermite polynomials.

Note that in the absence of an electric field ($v = 0$) the energy does not depend on k_y giving the characteristic large degeneracy of the Landau levels. Moreover, we then find in expression (19) the two energy scales mentioned in the introduction: 1) $\alpha_H = \alpha + \hbar\omega_0/2$, the energy in the LLL at $k_z = 0$ and 2) $\hbar\omega_0$ the energy spacing between levels. Since the temperature at which $\alpha_H = 0$ is where one expects the LLL modes to go critical within mean-field theory, it is taken to define the mean-field $H_{c2}(T)$ line.

Given the presence of the k_z^2 term in the energy, it is convenient to construct two c-axis length scales, one corresponding to each energy scale; they are

$$\xi_c = \left(\frac{\hbar^2}{2m_c\alpha_H}\right)^{1/2} \quad \text{and} \quad \ell_c = \left(\frac{\hbar}{m_c\omega_0}\right)^{1/2}. \tag{22}$$

The former is the standard mean-field c-axis correlation length, which is temperature dependent; while the latter is a c-axis version of the magnetic length

$$\ell_c = \left(\frac{m_{ab}}{m_c}\right)^{1/2} \ell, \tag{23}$$

which is temperature independent.

From the eigenstates and eigenvalues above we construct the following Green's function

$$\begin{aligned} G(\mathbf{r}, t; \mathbf{r}', t') = \Gamma \int \frac{d\omega}{2\pi} \int \frac{dk_y}{2\pi} \int \frac{dk_z}{2\pi}\, \exp\left\{ik_y(y-y') + ik_z(z-z') - i\omega(t-t')\right\} \\ \times \sum_{n=0}^{\infty} \frac{u_n\left(\frac{x}{\ell} - k_y\ell - i\tilde{k}_v\ell\right) u_n\left(\frac{x'}{\ell} - k_y\ell - i\tilde{k}_v\ell\right)}{\Gamma E_n(k_y, k_z) - i\omega}, \end{aligned} \tag{24}$$

where $\tilde{k}_v = m_{ab}v/\hbar^2\Gamma$. One might notice that when $v \neq 0$ the arguments of the u's are not complex conjugates with $x \leftrightarrow x'$; that is because the operator $\mathcal{H}$ is not Hermitian. The real issue is that eq. (14) is satisfied.

Various representations of $G(\mathbf{r}, t; \mathbf{r}', t')$ are useful depending on the calculation in question. Another useful form of $G(\mathbf{r}, t; \mathbf{r}', t')$ can be derived by performing the integral over ω and using the identity

$$\sum_{n=0}^{\infty} \frac{H_n(x) H_n(y)}{2^n n!} t^n = \frac{\mathrm{e}^{[2xyt - (x^2+y^2)t^2]/(1-t^2)}}{(1-t^2)^{1/2}}. \tag{25}$$

It leads to

$$\begin{aligned} G(\mathbf{r}, t; \mathbf{r}', t') = \frac{\Gamma}{4\pi\ell^2} \int \frac{dk_z}{2\pi} \left[\sinh\left[\frac{\Gamma\hbar\omega_0(t-t')}{2}\right]\right]^{-1} \exp\left\{-\Gamma\left[\frac{\hbar^2 k_z^2}{2m_c} + \frac{\hbar^2\tilde{k}_v^2}{2m_{ab}} + \alpha\right](t-t')\right\} \\ \exp\left\{-\coth\left[\frac{\Gamma\hbar\omega_0(t-t')}{2}\right] \frac{\left[(x-x')^2 + (y-y'+v(t-t'))^2\right]}{4\ell^2}\right\} \\ \exp\left\{\frac{i(x+x'-2i\tilde{k}_v\ell^2)(y-y'+v(t-t'))}{2\ell^2} + ik_z(z-z')\right\} \Theta(t-t'). \end{aligned} \tag{26}$$

In this form there is no longer any summation and the spatial dependence is simply that of a Gaussian, but the price paid is in the hyperbolic time dependence. One can see in the combination $(y - y' + v(t - t'))$ the tendency for the vortices to move in the negative y direction under the influence of the Lorentz force.

After the Green's function, the next quantity we will need is the correlation function $C(\mathbf{r}, t; \mathbf{r}', t') = \langle \Psi(\mathbf{r}, t)\ \Psi^*(\mathbf{r}', t') \rangle$. There are two complications here: the operator $\mathcal{H}$ is neither Hermitian nor translationally invariant. As a result some of the formulas relating C and G that we have become accustomed to are inappropriate; it is best to resort to the definitions. Substituting the expressions for $\Psi(\mathbf{r}, t)$ and $\Psi^*(\mathbf{r}', t')$ given by eq. (15) into the definition of $C(\mathbf{r}, t; \mathbf{r}', t')$ and performing the noise average yields

$$C(\mathbf{r}, t; \mathbf{r}', t') = \frac{2k_B T}{\Gamma} \int dt'' \int dr''\ G(\mathbf{r}, t; \mathbf{r}'', t'') G^*(\mathbf{r}', t'; \mathbf{r}'', t'') + O(\beta). \tag{27}$$

Many of the calculations that follow will use the Kubo formula in which there is no explicit electric field ($v = 0$). Then the expression for the correlator simplifies somewhat, becoming

$$\begin{aligned} C_{v=0}(\mathbf{r}, t; \mathbf{r}', t') = 2k_B T \Gamma \int \frac{d\omega}{2\pi} \int \frac{dk_y}{2\pi} \int \frac{dk_z}{2\pi}\ \exp\left\{ik_y(y - y') + ik_z(z - z') - i\omega(t - t')\right\} \\ \times \sum_{n=0}^{\infty} \frac{u_n\left(\frac{x}{\ell} - k_y\ell\right) u_n\left(\frac{x'}{\ell} - k_y\ell\right)}{\Gamma^2 E_n^2(k_z) + \omega^2}. \end{aligned} \tag{28}$$

Now let us move on to using these expressions to calculate the conductivity.

III. THE FLUCTUATION CONDUCTIVITY

Having the Green's function and correlation function, we are now ready to calculate the conductivity. We will focus on the conductivity due to fluctuations in the superconducting order parameter — the so-called Aslamazov-Larkin term. The normal contribution $\sigma^{(n)}$ must be included separately, and we are neglecting other possible contributions such as the Maki-Thompson or density-of-states terms.[25]

Recall that conductivities take on a form

$$\sigma \propto \frac{e^{*2}\, \mathcal{N}\, \tau}{m^*}, \tag{29}$$

where e^* and m^* are the effective charge and mass respectively, τ is a characteristic time scale, and $\mathcal{N}$ is the carrier density. Since we are interested in the conductivity due to superconducting fluctuations $\langle |\Psi|^2 \rangle$ will serve as the carrier density. An examination of the TDGL equation reveals that the kinetic coefficient Γ has dimensions $(energy \times time)^{-1}$; so that $time = (\Gamma \times energy)^{-1}$. The question then becomes: what is the appropriate energy scale? Thus far two candidates — α_H and $\hbar\omega_0$ — have emerged.

A. The direct approach

Now let us derive the flux-flow form of the uniform conductivity from a calculation with an explicit electric field applied. This approach has several advantages over the Kubo calculation. It extracts the conductivity from the current, a two-point object, instead of the current-current correlation function, a four-point object. Related to this point is the fact that many of the diagrams occurring in the Kubo calculation make canceling contributions. In addition, in the direct approach the $\alpha/\hbar\omega_0 \to 0$ limit (the LLL approximation) requires only LLL states, which is not true for the Kubo case. It can also be extended to include the nonlinear effects. (The advantage of the Kubo formalism is that it can be used to calculate the nonlocal conductivities $\sigma_{xx}(\mathbf{k})$ and $\sigma_{zz}(\mathbf{k})$.)

From equation (11) we see that the average current is obtained from the correlation function as follows

$$\langle J_x^{(s)}(\mathbf{r}, t) \rangle = \frac{\hbar e^*}{2i m_{ab}} \left(\frac{\partial}{\partial x} - \frac{\partial}{\partial x'} \right) C(\mathbf{r}, t; \mathbf{r}', t') \Bigg|_{(\mathbf{r}, t) = (\mathbf{r}', t')}. \tag{30}$$

We will drop the superscript (s) hereafter. At the lowest order in perturbation in theory, we can insert expression (27) into (30) to obtain

$$\langle J_x\rangle = \frac{k_B T\hbar e^*}{i\Gamma m_{ab}}\left(\frac{\partial}{\partial x}-\frac{\partial}{\partial x'}\right)\int dt''\int dr''\; G(\mathbf{r},t;\mathbf{r}'',t'')\; G^*(\mathbf{r}',t';\mathbf{r}'',t'')\Big|_{(\mathbf{r},t)=(\mathbf{r}',t')}. \tag{31}$$

We have verified a posteriori that in the direct approach the $\alpha/\hbar\omega_0 \to 0$ limit is equivalent to using only $n=0$ states from the start. Restricted to $n=0$ states, the Green's function becomes

$$G_0(\mathbf{r},t;\mathbf{r}',t') = \frac{\Gamma}{\sqrt{\pi}\ell}\int\frac{dk_y}{2\pi}\int\frac{dk_z}{2\pi}\;\exp\left\{ik_y(y-y')+ik_z(z-z')-\Gamma E_0(k_y,k_z)(t-t')\right\}$$
$$\times\exp\left\{-\frac{\left(\frac{x}{\ell}-k_y\ell-i\tilde{k}_v\ell\right)^2}{2}-\frac{\left(\frac{x'}{\ell}-k_y\ell-i\tilde{k}_v\ell\right)^2}{2}\right\}\;\Theta(t-t'). \tag{32}$$

Notice that the derivative with respect to x in eq. (31) pulls down a factor of $-(x/\ell^2-k_{y1}-i\tilde{k}_v)$, while that with respect to x' pulls down $-(x'/\ell^2-k_{y2}+i\tilde{k}_v)$. The wave vectors k_{y1} and k_{y2} will eventually prove to be equal (momentum conservation), so when $\mathbf{r}$ is set equal to $\mathbf{r}'$ we find

$$\langle J_x\rangle \;=\; \frac{\hbar e^*\tilde{k}_v}{m_{ab}}C_0(\mathbf{r},t;\mathbf{r},t) \;=\; \frac{e^{*2}E}{m_{ab}\Gamma\hbar\omega_0}\langle|\Psi_0|^2\rangle, \tag{33}$$

where $C_0(\mathbf{r},t;\mathbf{r},t)=\langle|\Psi_0|^2\rangle$ denotes the order-parameter fluctuations in the LLL. (Strictly speaking it is $\langle|\Psi_0|^2\rangle$ in the presence of the electric field, which is where the nonlinear effects would enter). Note that the conductivity has the expected form with the characteristic time given by $\tau = 1/\Gamma\hbar\omega_0$ and that any temperature dependence enters only through the carrier density and not through the characteristic time.

So far this result is for the lowest order in perturbation theory; however, all terms in the perturbative expansion for $C(\mathbf{r},t;\mathbf{r}',t')$ begin with some $G(\mathbf{r},t;\mathbf{r_1},t_1)$ and end with some $G^*(\mathbf{r}',t';\mathbf{r_n},t_n)$. It follows that the effect of taking the derivatives in eq. (30) will always be the same as it was above, and consequently, the flux-flow result, eq. (33), holds to all orders of perturbation theory in the LLL approximation. This result is remarkable in the simplicity of the relation between $\sigma_{xx}(\mathbf{0})$, a dynamic quantity, and $\langle|\Psi_0|^2\rangle$, a static quantity. One always expects the conductivity to be proportional to carrier density, but in this case the proportionality constant τ turns out to be rather trivial — having no temperature dependence.

B. The Kubo formalism

We now turn to the Kubo approach. For a system not too far from equilibrium the conductivity can be calculated from the Kubo formula

$$\sigma_{\mu\nu}(\mathbf{k},\omega) \;=\; \frac{1}{2k_BT}\int d(\mathbf{r}-\mathbf{r}')\int d(t-t')\;\mathrm{e}^{i\mathrm{k}\cdot(\mathrm{r}-\mathrm{r}')-i\omega(t-t')}\;\langle J^{(s)}_\mu(\mathbf{r},t)\;J^{(s)}_\nu(\mathbf{r}',t')\rangle_c\;, \tag{34}$$

where the suffix c denotes the "connected" piece and where this expression allows for a frequency dependence. The Kubo formula relates the conductivity, a dissipative quantity, to fluctuations in an associated quantity, here the superconducting current. As such, it is a version of a fluctuation-dissipation theorem. It calculates the linear response to an electric field without explicitly applying one; the fluctuations above are those in the absence of an electric field.

Inserting the expression for the current (11) into the Kubo formula (34) yields

$$\sigma_{\mu\nu}(\mathbf{k},\omega) \;=\; \frac{e^{*2}}{8k_BTm_\mu m_\nu}\int d(\mathbf{r}-\mathbf{r}')\int d(t-t')\;\mathrm{e}^{i\mathrm{k}\cdot(\mathrm{r}-\mathrm{r}')-i\omega(t-t')}$$
$$\left(P_{1\mu}+P^*_{2\mu}\right)\left(P_{3\nu}+P^*_{4\nu}\right)\;\langle\Psi(\mathbf{r_1},t)\Psi^*(\mathbf{r_2},t)\Psi(\mathbf{r_3},t')\Psi^*(\mathbf{r_4},t')\rangle_c\Big|_{\substack{\mathbf{r_1}=\mathbf{r_2}=\mathbf{r}\\ \mathbf{r_3}=\mathbf{r_4}=\mathbf{r}'}}. \tag{35}$$

One can see that calculated in this way the conductivity is a four-point object as mentioned in the introduction. Henceforth, we will consider DC results ($\omega=0$) only and will drop the frequency dependence from our expressions.

The aim now is to calculate averages of the sort $\langle\Psi(\mathbf{r_1},t_1)\Psi^*(\mathbf{r_2},t_2)\Psi(\mathbf{r_3},t_3)\Psi^*(\mathbf{r_4},t_4)\rangle_c$. At the lowest order in perturbation theory (the Gaussian term); one simply applies Wick's theorem

$$\langle \Psi(\mathbf{r_1},t)\Psi^*(\mathbf{r_2},t)\Psi(\mathbf{r_3},t')\Psi^*(\mathbf{r_4},t')\rangle_c = \langle \Psi(\mathbf{r_1},t)\Psi^*(\mathbf{r_4},t')\rangle\langle \Psi(\mathbf{r_3},t')\Psi^*(\mathbf{r_2},t)\rangle, \tag{36}$$

retaining only the connected piece. The Gaussian term is represented diagrammatically in Figure 1. An arrow corresponds to a Green's function, and a circle corresponds to the noise average. The combination arrow-circle-arrow constitutes a correlation function. Hence the conductivity at Gaussian order requires two correlation functions. Not drawn but of crucial importance are the momentum operators acting at sites $(\mathbf{r},t)$ and $(\mathbf{r}',t')$ that make it a current-current correlator instead of a density-density correlator.

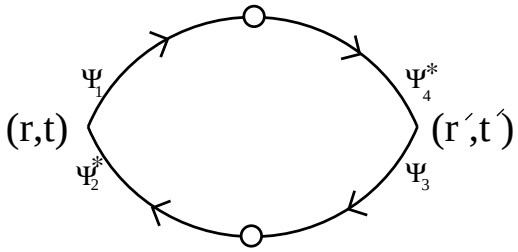

FIG. 1. Gaussian order diagram for the conductivity. An arrow corresponds to a Green's function, and a circle corresponds to the noise average. Not drawn but of crucial importance are the momentum operators acting at sites $(\mathbf{r},t)$ and $(\mathbf{r}',t')$.

Let us focus our attention for now on the uniform dc conductivities $\sigma_{xx}(\mathbf{0})$ and $\sigma_{zz}(\mathbf{0})$. Calculated in the LLL approximation and to Gaussian order they are

$$\sigma_{xx}^{(G)}(\mathbf{0}) = \frac{e^{*2}\ \langle|\Psi_0|^2\rangle}{m_{ab}}\left(\frac{1}{\Gamma\hbar\omega_0}\right) \tag{37}$$

and

$$\sigma_{zz}^{(G)}(\mathbf{0}) = \frac{e^{*2}\ \langle|\Psi_0|^2\rangle}{m_{c}}\left(\frac{1}{8\Gamma\alpha_H}\right) \tag{38}$$

We see here the characteristic time of the ab-plane conductivity is $\tau_{ab} = 1/\Gamma\hbar\omega_0$ while that corresponding to the c-axis conductivity is $\tau_c = 1/8\Gamma\alpha_H$.

Consider now how the Kubo formula reproduced the flux-flow result at Gaussian order. First of all the momentum operators intrinsic to $\sigma_{xx}(\mathbf{0})$ act like creation or annihilation operators raising or lowering the Landau level with the result that one of the Ψ's at $(\mathbf{r},t)$ is in a higher level; the same thing happening at $(\mathbf{r}',t')$ as well. Consequently, in the LLL limit, we have one $n=0$ correlator and one $n=1$ correlator. With this in mind, we now look at the time integral in the Kubo formula, which becomes

$$\int d(t-t')\ \exp\left\{-\Gamma\left[E_0(k_{z1})+E_1(k_{z2})\right]|t-t'|\right\}, \tag{39}$$

where k_{z1} and k_{z2} are the z components of momentum running through the $n=0$ and $n=1$ channels, respectively. (Actually $k_{z1}=k_{z2}$ by momentum conservation.) Because $E_0(k_{z1})$ is much smaller than $E_1(k_{z2})$ we can drop $E_0(k_{z1})$ from the integrand above. This last step is equivalent to using a static (equilibrium) $n=0$ correlator and hence produces a relation between the dynamic conductivity and the static density. In fact, the integral yields simply a factor $1/\Gamma\hbar\omega_0$ — the characteristic time in the flux-flow formula. The flux-flow formula obtained in the direct approach above suggests that the Gaussian density $\langle|\Psi_0|^2\rangle$ should be replaced by the fully renormalized density $\langle|\tilde{\Psi}_0|^2\rangle$ but that the characteristic time $\tau_{ab}=1/\Gamma\hbar\omega_0$ should remain as is. The way to produce this result within the Kubo formalism is to renormalize the $n=0$ correlator while leaving the $n=1$ correlator essentially untouched. If this is true then diagrams that dress up or otherwise disrupt the bare $n=1$ correlator should have no overall effect.

C. The Hartree-Fock Approximation

Our first attack on going beyond Gaussian order, *i.e.* incorporating the nonlinear terms, will be the Hartree-Fock approximation. At Gaussian order the superconducting fluctuations are

$$\langle|\Psi_0|^2\rangle = \frac{k_BT}{4\pi\ \alpha_H\ \xi_c\ell^2}, \tag{40}$$

which would seem to imply that the conductivity diverges at mean-field H_{c2} ($\alpha_H = 0$). This seeming divergence is eliminated when one adopts the Hartree or Hartree-Fock approximation.[21,26]

From the perturbation theory for Ψ (17) we can obtain the series for $\langle \Psi(\mathbf{r_1}, t)\Psi^*(\mathbf{r_2}, t)\Psi(\mathbf{r_3}, t')\Psi^*(\mathbf{r_4}, t')\rangle$ and in turn the series for the conductivity. The new diagrammatic feature is a "quartic" vertex at which four lines meet with two arrows pointing in and two pointing out. Two diagrams occurring at the first order in β are shown in Figure 2. Because of the structure of the conductivity, especially the momentum operators acting at $(\mathbf{r}, t)$ and $(\mathbf{r}', t')$, the diagram shown in Fig. 2(b) has zero contribution at $\mathbf{k} = \mathbf{0}$ for both σ_{xx} and σ_{zz}.

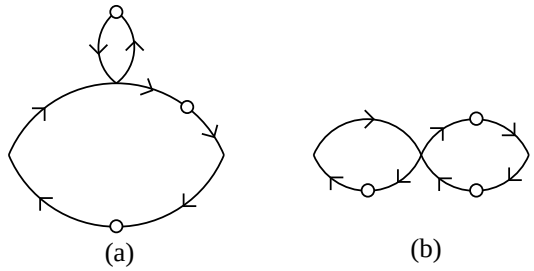

FIG. 2. Diagrams with one quartic vertex. Diagram 2(a) is included in the Hartree-Fock resummation. Diagram 2(b) has zero contribution at $\mathbf{k} = \mathbf{0}$ and is "down" in the calculation of $\sigma_{xx}(\mathbf{k} \neq \mathbf{0})$.

Diagrams like that in Fig. 2(a) can be resummed by replacing α_H with $\tilde{\alpha}$, where $\tilde{\alpha}$ is defined self-consistently as $\tilde{\alpha} = \alpha_H + 2\beta\langle|\tilde{\Psi}_0|^2\rangle$, where what we mean here by $\langle|\tilde{\Psi}_0|^2\rangle$ is $\langle|\Psi_0|^2\rangle$ (eq. (40) with $\alpha_H \to \tilde{\alpha}$; all of which leads to

$$\tilde{\alpha} = \alpha_H + \frac{\beta\ k_B T}{2\pi\ \ell^2 \xi_c\ \tilde{\alpha}}. \tag{41}$$

Replacing α_H with $\tilde{\alpha}$ constitutes a resummation, the Dyson equation for which is represented diagrammatically in Fig. 3. It corresponds to a renormalization of the Green's function.

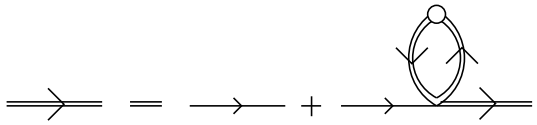

FIG. 3. Diagrammatic representation of the Hartree-Fock approximation. The double lines represent renormalized Green's functions; the single lines represent bare Green's functions.

In analogy with many-body physics, this replacement is called the Hartree-Fock (HF) approximation as it takes into account both the direct and exchange terms. In addition to eliminating a large number of graphs from the perturbation theory; the HF resummation replaces α_H which can be zero or negative with $\tilde{\alpha}$ which cannot — curing the divergence problem mentioned above. The removal of the divergence is connected to the fact that a large magnetic field effectively reduces the dimension of the problem by two.[27] Moreover, the HF approximation goes a long way toward achieving agreement with measured conductivities.[28] This success suggests that the same philosophy ($\alpha_H \to \tilde{\alpha}$) should be adopted when considering where the LLL approximation is valid. In the HF approximation $\alpha_H \to \tilde{\alpha}$ while $\hbar\omega_0$ remains the same. So whereas it originally appeared that the LLL approximation was valid near the mean-field $H_{c2}(T)$ line where α_H is small, it would now appear to be valid where $\tilde{\alpha}$ is small. But as already noted $\tilde{\alpha}$ does not change sign, it grows small only as α_H grows large and negative, *i.e.* below the mean-field $H_{c2}(T)$ line. Ikeda[16] has investigated renormalization effects beyond HF, finding that they are merely refinements to the HF considerations, suggesting that the LLL approximation has a substantial region of validity within the vortex-liquid regime.

If we replace α_H with $\tilde{\alpha}$ in the Gaussian conductivities and look in the limit of $\alpha_H \ll 0$ we find that

$$\lim_{\alpha_H \ll 0}\ \sigma_{xx}(\mathbf{0}) = \frac{e^*|\alpha_H|}{2\beta\hbar B\Gamma}. \tag{42}$$

Note that $\sigma_{xx}(\mathbf{0})$ at this level of approximation already shows many of the features seen in the experiments in the vortex-liquid regime: the *resistivity* is linear in B with a zero intercept and extrapolates to the normal resistivity at the mean-field $H_{c2}(T)$ line, as can be seen for instance in the Fendrich *et al.* data prior to irradiation.[14]

D. Beyond the Hartree-Fock Approximation

While the Hartree or HF approximation goes along way toward describing certain properties such as the specific heat, it is totally inadequate for examining other features, such as the extent of crystalline ordering within the ab plane. A much more sophisticated approach, such as the Parquet resummation[29], is needed for that. We do not provide such a scheme here, instead we examine a few diagrams beyond the HF approximation. We will find a cancellation among most of these diagrams at $\mathbf{k} = \mathbf{0}$ suggesting that the Hartree approximation is already quite good for the uniform conductivity. The absence of this cancellation at $\mathbf{k} \neq \mathbf{0}$, on the other hand, suggests the need to go beyond Hartree theory when considering the nonlocal effects.

As we are now considering a perturbation theory about the HF approximation, the series is no longer a power series in β. Rather it is a power series in x where

$$x = \frac{\beta k_B T}{16\pi\ell^2 \xi_c \tilde{\alpha}^2}, \tag{43}$$

the dimensionless parameter introduced by Ruggeri and Thouless.[27] The self-consistent equation above, eq. (41), is now rather compactly written as

$$\alpha_H = \tilde{\alpha}(1 - 8x). \tag{44}$$

In the expansion of the uniform conductivity $\sigma_{xx}(\mathbf{0})$ there are no contributions of $O(x)$. Recall that of the diagrams at order β (Fig. 2) there are those of the HF type which have been absorbed into $\tilde{\alpha}$, and the others make no contribution at $\mathbf{k} = \mathbf{0}$. Some diagrams contributing to the conductivity at $O(x^2)$ are shown in Figures 4, 5 and 6.

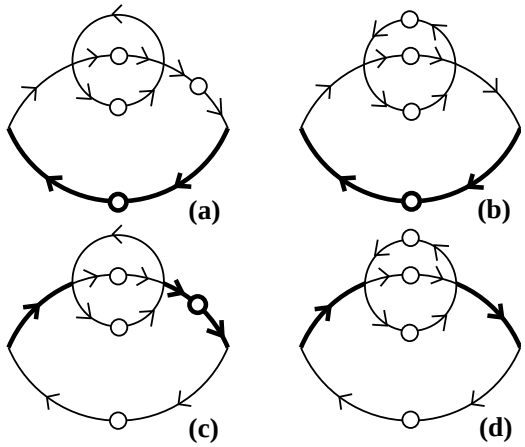

FIG. 4. Diagrams contributing to σ_{xx} at order x^2. The bold lines indicate $n \geq 1$ Green's functions; the thin lines $n = 0$ Green's functions. Diagrams (a) and (c) are Green's function renormalizing; while (b) and (d) are noise-renormalizing — the difference being in the placement of the circles (noise averages). Diagrams (a) and (b) contribute to the flux-flow formula, (c) is "down" and does not contribute to the LLL approximation, and (d) is canceled by another diagram at $\mathbf{k} = \mathbf{0}$.

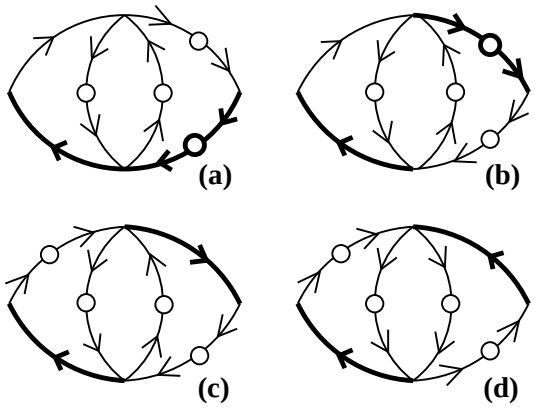

FIG. 5. Vertex renormalizing diagrams contributing to σ_{xx} at order x^2. Diagrams (a) and (b) are "down;" diagram (c) is zero at $\mathbf{k} = \mathbf{0}$; and (d) is canceled by the diagram in Fig. 4 (d).

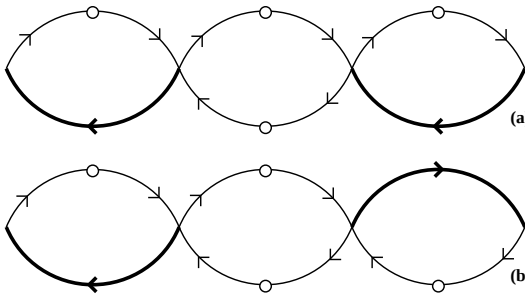

FIG. 6. More vertex renormalizing diagrams contributing to σ_{xx} at order x^2. These diagrams do not contribute at $\mathbf{k} = \mathbf{0}$.

There are a number of considerations in addition to the usual ones of the topology and degeneracy to keep in mind when enumerating and evaluating the diagrams that occur in the perturbation series for σ_{xx}. Because the conductivity is a dynamic quantity, there is the distinction between Green's functions and correlation functions to bear in mind. We make this differentiation by including a small circle representing the noise average in the middle of a correlation function. Diagrams may differ in the placement of circles; for example, compare Figs. 4(a) and (b) or Figs 5(b) and (c). In addition, because the order parameter is complex, the Green's function carries a direction, indicated by the arrow. Hence diagrams may be distinguished by the placement of arrows around the diagram; for instance, compare Figs. 5(c) and (d). Also because the order parameter is expanded in Landau levels, the Landau level of each line is another consideration. We make this differentiation by putting the higher Landau-level Green's functions in bold. So diagrams may differ in Landau level structure; for example, compare Figs. 4(a) and (c) or Figs. 5(a) and (b). On the other hand, in the evaluation of $\sigma_{zz}(\mathbf{0})$ all of the Green's functions are in the LLL.

Recall that at Gaussian order $\sigma_{xx}(\mathbf{0})$ has one correlation function and thus two Green's functions in the $n = 1$ state. It turns out that at all orders in perturbation theory the diagrams contributing to the LLL approximation have a maximum of two higher-Landau-level Green's functions. So diagrams like that in Fig. 4(c) and those in Figs. 5 (a) and (b) are "down" by a factor of $\tilde{\alpha}/\hbar\omega_0$ and are not included to this order of approximation. Of the remaining diagrams it has been argued that those which have a simple $n = 1$ correlator (*e.g.* Figs. 4(a) and (b)) contribute to the flux-flow result and that the others (*e.g.* Figs. 4(d), 5(c) and (d) and 6(a) and (b)) must have a combined contribution of zero at $\mathbf{k} = \mathbf{0}$. When we evaluated these diagrams, we indeed found that the diagram in Figs. 5(c), 6(a) and 6(b) gave no contribution at $\mathbf{k} = \mathbf{0}$ and that the contributions due to the diagrams in Figs. 4(d) and Figs. 5(d) were equal and opposite. We will demonstrate this explicitly in the $2D$ case.

The diagrams in Fig. 4(a) and (c) renormalize the Green's function, and those in Fig. 4(b) and (d) renormalize the noise. The diagrams in Figs. 5 and 6 renormalize the quartic vertex. Note that on the $n = 1$ side, the Green's function renormalizing diagram was down whereas the noise renormalizing diagram was not. A similar phenomenon occurs when we consider the effect of disorder.

IV. WAVE-VECTOR DEPENDENCE

Now let us turn to the nonlocal, **k**-dependent, conductivity. In some instances we calculate the full **k**-dependence[9], while in others we restrict our attention to the coefficients in a small-**k** expansion

$$\sigma_{\mu\nu}(\mathbf{k}) \;=\; \sigma_{\mu\nu}(\mathbf{0}) \;+\; S_{\mu\alpha\beta\nu}\; k_\alpha k_\beta + O(k^4). \tag{45}$$

The coefficients $S_{\mu\alpha\beta\nu}$ and the associated length scales can be related to the vortex picture. Since the vortices move in the y direction when the electric field and current are in the x direction, S_{xxxx} is associated with shearing[8] and S_{xyyx} with compression. S_{xzzx} is related to the "integrity" of vortices (Huse and Majumdar[7] call it the "tilt viscosity").

A. The Gaussian results

The small wave-vector expansion of the conductivity at Gaussian order (within the combined HF and LLL approximations) is

$$\sigma_{xx}^{(G)}(\mathbf{k}) = \sigma_{xx}^{(G)}(\mathbf{0})\left[1 - \frac{\ell^2 k_x^2}{4} + \frac{3\hbar^2\omega_0^2\ell^2 k_y^2}{64\tilde{\alpha}^2} - \ell_c^2 k_z^2 + O(k^4)\right], \tag{46}$$

where we have factored out $\sigma_{xx}^{(G)}(\mathbf{0})$. First note that S_{xxxx} and S_{xzzx} are negative, *i.e.* they have the sign that cannot be handled using the hydrodynamic approach. Furthermore, the length scales multiplying k_y^2 and k_z^2 are magnetic lengths, *i.e.* they have no temperature dependence.

It is easy to see why (calculationally) the c-axis length scale in the Gaussian calculation of $\sigma_{xx}^{(G)}$ is ℓ_c. The z-dependence has no effect on the Landau level structure; therefore, it remains true that $\sigma_{xx}(k_z)$ is comprised of one $n=0$ and one $n=1$ correlator. We can take advantage of the disparity in "masses" ($\tilde{\alpha} \ll \hbar\omega_0$) by insisting that the external momentum k_z be sent through the $n=1$ channel. (This choice does not affect the outcome, it just makes it more apparent.) The internal momentum integral is dominated by the smallest poles, which are those associated with $\tilde{\alpha}$, and the terms involving k_z and $\hbar\omega_0$ are left essentially intact. The full k_z dependence at Gaussian order is thus

$$\sigma_{xx}^{(G)}(k_z) = \sigma_{xx}^{(G)}(\mathbf{0})\left[1 + k_z^2\ell_c^2/2\right]^{-2}, \tag{47}$$

where the structure is simply that of $[E_1(k_z)]^{-2}$ with $\tilde{\alpha} \to 0$.

The Landau level structure of S_{xxxx} is slightly different. This time one correlator is in the $n=0$ level while the other is in either the $n=1$ or the $n=2$ level. For an expansion in k_x^2 each additional power of k_x^2 requires one higher Landau level. But the important point is that there is no contribution with two $n=0$ correlators. The k_x dependence at Gaussian order is

$$\sigma_{xx}^{(G)}(k_x) = \sigma_{xx}^{(G)}(\mathbf{0})\left[\frac{1 - e^{-k_x^2\ell^2/2}}{k_x^2\ell^2/2}\right]. \tag{48}$$

The combined k_x and k_z dependences are given by

$$\sigma_{xx}^{(G)}(k_x,k_z) = \sigma_{xx}^{(G)}(\mathbf{0})\left[\mathrm{e}^{-k_x^2\ell^2/2}\sum_{n=0}^{\infty}\frac{(n+1)\left(k_x^2\ell^2/2\right)^n}{n!\left[(n+1) + k_z^2\ell_c^2/2\right]^2}\right]. \tag{49}$$

As opposed to S_{xxxx} and S_{xzzx}, S_{xyyx} is positive at Gaussian order. In fact if we had included the next term in the $\tilde{\alpha}/\hbar\omega_0$ expansion we would see that S_{xyyx} changes sign as T is lowered.[8] As T decreases the associated length scale associated with S_{xyyx}, $\xi_\perp \propto \hbar\omega_0\ell/\tilde{\alpha}$, increases. A T-dependent length scale here is somewhat surprising. In the vortex picture S_{xyyx} appears to be related to compression, but one might expect that the compressibility to be pretty much the same for the liquid and the solid, and so relatively T-independent. The Gaussian calculation is in conflict with this expectation. If this length scale found in the transverse conductivity does indeed increase as T decreases, it will prove interesting to compare it to similar growing ab-plane length scales, for example, the phase coherence length and the length over which density-density fluctuations decay[30], which recent Monte Carlo simulations suggest grow in the same way[31].

In the scenario in which we apply current and wish to extract the voltage distribution, it is the characteristic lengths of the resistivity which are important. This is why the signs of the S's are so crucial. They determine the pole structure of the nonlocal resistivity $\rho(\mathbf{k})$ and consequently the length scales of $\rho(\mathbf{r})$. Consider, as an example, a c-axis conductivity of the form

$$\sigma_{zz}(k_z) = \sigma_{zz}^{(n)} + \sigma_{zz}^{(s)}(0) + S_{zzzz}k_z^2 + O(k^4), \tag{50}$$

where a local normal conductivity has been included. If S is positive, the hydrodynamic approach[7] yields a length scale $[S/(\sigma^{(s)}+\sigma^{(n)})]^{1/2}$. If S is negative, a Padé approximant approach[9] produces a length scale $[\sigma^{(n)}|S|/\sigma^{(s)}(\sigma^{(s)}+\sigma^{(n)})]^{1/2}$ which is much smaller than the previous one because of the factor $(\sigma^{(n)}/\sigma^{(s)})^{1/2}$. Returning to the case of S_{xyyx}, if it were to change sign from positive to negative as more diagrams are included, the associated length scale would then be short which may be consistent with the expectations of the vortex picture. With such dramatic consequences regarding the nonlocal behavior of the resistivity, one might expect that changes in the signs of the S's would have experimental signatures.

The difference between S_{xyyx} and the others is that all four Ψ's in the calculation of S_{xyyx} can be in the LLL. Applying the definition of S_{xyyx}, namely

$$S_{xyyx} = \frac{1}{2}\frac{\partial^2\sigma_{xx}(\mathbf{k})}{\partial k_y^2}\bigg|_{\mathbf{k}=\mathbf{0}}, \tag{51}$$

to the Kubo formula (eq. (35)) and restricting to LLL states yields

$$\begin{aligned} S_{xyyx} \;=\; -\frac{e^{*2}}{16k_BTm_{ab}^2}\int d(\mathbf{r}-\mathbf{r}')\int d(t-t')\;(y-y')^2\Big(P_{1x}+P_{2x}^*\Big)\Big(P_{3x}+P_{4x}^*\Big) \\ \langle\Psi_0(\mathbf{r_1},t)\Psi_0^*(\mathbf{r_2},t)\Psi_0(\mathbf{r_3},t')\Psi_0^*(\mathbf{r_4},t')\rangle_c\Big|_{\substack{\mathbf{r_1}=\mathbf{r_2}=\mathbf{r}\\ \mathbf{r_3}=\mathbf{r_4}=\mathbf{r}'}}. \end{aligned} \tag{52}$$

This expression involves only LLL states is hence accessible to simulations and other methods which use only LLL states.[32]

Another quantity that involves only LLL states is the c-axis conductivity, $\sigma_{zz}(\mathbf{k})$, at Gaussian order it is

$$\sigma_{zz}^{(G)}(\mathbf{k}) = \sigma_{zz}^{(G)}(\mathbf{0})\left[\mathrm{e}^{k_\perp^2\ell^2/2}\left(\frac{1-(1+k_z^2\xi_c^2/4)^{-1/2}}{k_z^2\xi_c^2/8}\right)\right], \tag{53}$$

where $k_\perp^2 = k_x^2 + k_y^2$. Since the calculation involves only $n=0$ states, the c-axis length scale is necessarily ξ_c. If this result is expanded one finds that none of S's has the sign required by the hydrodynamic approach.

B. Beyond Gaussian

As already mentioned the HF approximation is inadequate for determining the extent of crystal ordering within the ab plane and as such is also inadequate for examining shear effects. To see if S_{xxxx} has a long length scale or changes sign at low T, we must look beyond the HF approximation. The same is true of S_{xzzx}.

We argued that the uniform conductivity, $\sigma_{xx}(\mathbf{k}=\mathbf{0})$, could be obtained from the subset of diagrams that renormalize the $n=0$ correlator and leave the $n=1$ untouched beyond the HF resummation. In the LLL limit the fully renormalized $n=0$ correlator $\tilde{C}_{n=0}(\mathbf{r},t;\mathbf{r}',t')$ has *exactly* the same dependence on x, x', y and y' as its "bare" version; thus, the k_x-dependence of this particular resummation is exactly the same as that in the Gaussian calculation (eq. (48)). Furthermore, the external momentum k_z can still be sent through the $n=1$ channel, yielding again the dependence seen in the Gaussian calculation (eq. (47)). Resumming this subset of diagrams only alters the magnitude $\sigma_{xx}(\mathbf{0})$; the k_x and k_z dependence remain the same as they were in the Gaussian calculation, *i.e.*

$$\sigma_{xx}^{(FF)}(k_x,k_z) = \sigma_{xx}(\mathbf{0})\left[\mathrm{e}^{-k_x^2\ell^2/2}\sum_{n=0}^{\infty}\frac{(n+1)\left(k_x^2\ell^2/2\right)^n}{n!\left[(n+1)+k_z^2\ell_c^2/2\right]^2}\right]. \tag{54}$$

where

$$\sigma_{xx}(\mathbf{0}) = \frac{e^{*2}\langle|\tilde{\Psi}_0|^2\rangle}{m_{ab}\Gamma\hbar\omega_0} \tag{55}$$

and where

$$\langle|\tilde{\Psi}_0|^2\rangle = \frac{k_B T}{4\pi\ \tilde{\alpha}\ \xi_c \ell^2}\left[1 + O(x^2)\right]. \tag{56}$$

So for this particular subset of diagrams, we only have to do the perturbative expansion for the static quantity $\langle|\tilde{\Psi}_0|^2\rangle$. Consequently, if S_{xxxx} and S_{xzzx} are going to change sign at low T and give long length scales, then other diagrams, such as the vertex-renormalizing diagrams (see Fig. 5), must be important.

Recall that in the $\tilde{\alpha} \ll \hbar\omega_o$ limit we only want diagrams with at most two higher Landau level ($n \geq 1$) Green's functions. Green's functions meeting at a noise average must be in the same Landau level; while those meeting at a vertex can be in different Landau levels. So either the two $n \geq 1$ Green's functions meet each other at a noise average, or each meets three $n = 0$ Green's functions at a vertex. Otherwise, there will be at least three higher Landau level Green's functions; see for example, Fig. 4(c). We have already considered those diagrams in which the two $n \geq 1$ Green's functions meet each other at a noise average — they are the ones that yield the flux-flow result $\sigma_{xx}^{(FF)}(\mathbf{k})$ — they are also essentially two-point quantities and thus do not probe viscous effects such as shearing.

Let us find an expression for those terms in which each $n \geq 1$ Green's functions meets a vertex. Recall the TDGL equation in symbolic form $\Psi_1 = G_{1,2}\eta_2 - \beta G_{1,2}\Psi_2^*\Psi_2\Psi_2$ (eq. (16)). Of the four Ψ's in the Kubo formula, let us replace the two that are in higher Landau levels with the second term on the right hand side of eq. (16). This substitution yields

$$\begin{aligned}\Sigma_{xx}(k_x,k_z) = \frac{e^{*2}\beta^2}{8k_B T m_{ab}^2}\int d(\mathbf{r}-\mathbf{r}')\int d(t-t')\int_5\int_6 \mathrm{e}^{ik_x(x-x')+ik_z(z-z')} \\ \Big(P_{1x}+P_{2x}^*\Big)\Big(P_{3x}+P_{4x}^*\Big)\Big\{G_{2,5}^*G_{3,6}\langle\Psi_1\Psi_5^*\Psi_5^*\Psi_5\Psi_6\Psi_6\Psi_6^*\Psi_4^*\rangle_c \\ +G_{2,5}^*G_{4,6}^*\langle\Psi_1\Psi_5^*\Psi_5^*\Psi_5\Psi_6^*\Psi_6^*\Psi_6\Psi_3\rangle_c + c.c.\Big\}\Big|_{\substack{1=2=(\mathbf{r},t)\\3=4=(\mathbf{r}',t')}}.\end{aligned} \tag{57}$$

In this symbolic notation, the numbers denote points in space-time, *e.g.* $5 \to (\mathbf{r_5}, t_5)$. This expression factors out the "bare" $n \geq 1$ Green's functions explicitly, leaving averages which involve LLL states only. The LLL average is a rather complicated eight-point object, but in principle, coupled with eqs. (49) and (52), it allows one to find the conductivity from simulations that use only LLL states. Because the Green's functions that have been factored out involve higher Landau level states, they are rather short-ranged in both time and space. When investigating a regime in which one expects the LLL object to become long-ranged, it is tempting to approximate the Green's function by some appropriately scaled delta function $\delta(\mathbf{r}-\mathbf{r}')\delta(t-t')$ after the derivatives have acted.

In the next section we will provide some explicit expressions for the diagrams in Figs. 4, 5 and 6 for the two-dimensional case. But before leaving this section, let us make one point about the k_z behavior. As previously mentioned the diagrams 4(d) and 5(d) cancel at $k_z = 0$, but note that in these diagrams there is no longer an $n = 1$ channel through which we can pass the external momentum k_z. Therefore, one might expect that one picks up the ξ_c length scale instead of ℓ_c, however, this is not the case. Just as these diagrams cancel at $\mathbf{k} = \mathbf{0}$ so do the leading terms (*i.e.* the $k_z^2\xi_c^2$ terms) in the k_z expansion.

V. TWO-DIMENSIONAL RESULTS

Many of the results above hold for films and even simplify in this case. The uniform conductivity is still given by the flux-flow formula in the LLL approximation. The diagrammatic structure of the perturbation series is exactly the same; and which diagrams are down and so forth also carries through; only the evaluation of the diagrams changes.

To do these calculations we will of course need the $2D$ Green's function, which in the absence of an electric field is

$$G_{2D}(\mathbf{r},t;\mathbf{r}',t') = \frac{\Gamma}{L_z}\int\frac{d\omega}{2\pi}\int\frac{dk_y}{2\pi}\mathrm{e}^{-i\omega(t-t')+ik_y(y-y')}\sum_{n=0}^{\infty}\frac{u_n\left(\frac{x}{\ell}-k_y\ell\right)u_n\left(\frac{x'}{\ell}-k_y\ell\right)}{\Gamma E_n - i\omega}, \tag{58}$$

where $E_n = \alpha + \hbar\omega_0(n+1/2)$ and L_z is the film thickness. The Gaussian result for the conductivity is

$$\sigma_{xx}(\mathbf{k}) = \frac{e^{*2}\langle|\tilde{\Psi}_0|^2\rangle_{2D}}{m_{ab}\Gamma\hbar\omega_0}\left[1 - \frac{\ell^2 k_x^2}{4} + \frac{\hbar^2\omega_0^2\ell^2 k_y^2}{8\tilde{\alpha}_{2D}^2} + O(k^4)\right] \tag{59}$$

in the LLL limit. Other than a different numerical coefficient in front of the k_y^2 (S_{xyyx}), the result is similar to the $3D$ result (eq. (46)). Again we are applying the HF approximation so that $\tilde{\alpha} = \alpha_H + 2\beta\langle|\tilde{\Psi}_0|^2\rangle$ where

$$\langle|\tilde{\Psi}_0|^2\rangle_{2D} = \frac{k_B T}{2\pi\ \tilde{\alpha}_{2D}\ L_z\ell^2}, \tag{60}$$

which leads to the self-consistent equation

$$\tilde{\alpha}_{2D} = \alpha_H - \frac{\beta\ k_B T}{\pi\ \ell^2 L_Z\ \tilde{\alpha}_{2D}}. \tag{61}$$

The expansion parameter in the two-dimensional perturbation series is

$$x_{2D} = \frac{\beta\ k_B T}{4\pi\ \ell^2 L_z\ \tilde{\alpha}_{2D}^2}, \tag{62}$$

allowing one to re-express eq. (61) as $\alpha_H = \tilde{\alpha}_{2D}(1 - 4x_{2D})$.[27]

Evaluating some of the diagrams in Figs. 4 and 5 gives

$$\sigma_{xx}^{(FF)} = \sigma_{xx}^{(G)}(\mathbf{0})\ \frac{7x_{2D}^2}{2}\ \left[\mathrm{e}^{-k_\perp^2\ell^2/2}\left(1 - k_y^2\ell^2 + \frac{1}{4}k_y^2k_\perp^2\ell^4\right)\right] \tag{63}$$

$$\sigma_{xx}^{4(d)} = \sigma_{xx}^{(G)}(\mathbf{0})\ \frac{x_{2D}^2}{4}\ \left[\mathrm{e}^{-k_\perp^2\ell^2/2}\left(1 - k_y^2\ell^2 + \frac{1}{4}k_y^4\ell^4 + k_x^2k_y^2\ell^4\right)\right] \tag{64}$$

$$\sigma_{xx}^{5(c)} = \sigma_{xx}^{(G)}(\mathbf{0})\ \frac{x_{2D}^2}{8}\ \left[\mathrm{e}^{-3k_\perp^2\ell^2/4}\left(-k_x^2\ell^2 + k_y^2\ell^2 - k_y^2k_\perp^2\ell^4 + \frac{1}{4}k_y^2k_\perp^4\ell^6\right)\right] \tag{65}$$

$$\sigma_{xx}^{5(d)} = \sigma_{xx}^{(G)}(\mathbf{0})\ \frac{x_{2D}^2}{4}\ \left[\mathrm{e}^{-k_\perp^2\ell^2}\left(-1 + k_x^2\ell^2 + 2k_y^2\ell^2 - \frac{5}{4}k_y^2k_\perp^2\ell^4 + \frac{1}{4}k_y^2k_\perp^4\ell^6\right)\right] \tag{66}$$

$$\sigma_{xx}^{6(a)} = \sigma_{xx}^{(G)}(\mathbf{0})\ 2x_{2D}^2\ \left[\mathrm{e}^{-3k_\perp^2\ell^2/2}\left(k_\perp^2\ell^2 - k_y^2k_\perp^2\ell^4 + \frac{1}{4}k_y^2k_\perp^4\ell^6\right)\right] \tag{67}$$

$$\sigma_{xx}^{6(b)} = \sigma_{xx}^{(G)}(\mathbf{0})\ 2x_{2D}^2\ \left[\mathrm{e}^{-3k_\perp^2\ell^2/2}\left(-k_x^2\ell^2 + k_y^2\ell^2 - k_y^2k_\perp^2\ell^4 + \frac{1}{4}k_y^2k_\perp^4\ell^6\right)\right]. \tag{68}$$

These calculations were done with the Green's function shown in bold in the figures in the $n = 1$ state. Recall that if we are interested in S_{xyyx} we must redo the calculation with all $n = 0$ states, and if we are interested in S_{xxxx} we must also add to the expressions above those with $n = 2$ Green's functions. Here our interest is in showing explicitly the overall null contribution of these diagrams at $\mathbf{k} = \mathbf{0}$ — whether it be that the individual diagrams have zero contribution (*e.g.* diagrams 5(c), 6(a) and 6(b)) or that diagrams cancel (*e.g.* diagrams 4(d) and 5(d)) — and to suggest that the same does not apply at $\mathbf{k} \neq \mathbf{0}$.

VI. DISORDER

Disorder introduces competing effects: it provides pinning centers which may couple to the viscous effects even at $\mathbf{k} = \mathbf{0}$, but it also disrupts the growth in crystalline order which yields the viscous effects in the first place. With translational invariance destroyed, the flux-flow formula no longer applies. We will examine the effects of disorder at low order in perturbation theory within the Kubo formalism.

We can in principle take the direct approach at $\mathbf{k} = \mathbf{0}$ using the Green's functions with the explicit electric field applied. However, it is more complicated than it was in the absence of disorder. We confirmed for the pure system that we could use solely $n = 0$ states from the outset. So long as the electric field was explicitly applied, taking the $\tilde{\alpha}/\hbar\omega_0 \to 0$ limit in the beginning (*i.e.* using Green's functions with only $n = 0$ states) or at the end yielded the same results. However, the same is not true in the presence of disorder. The time integrals here are more involved, and taking the $\tilde{\alpha}/\hbar\omega_0 \to 0$ limit in the beginning and at the end gives different results. With this complication, the direct approach is no better than using the Kubo formalism.

A. Point disorder

In the experiments by Fendrich *et al.*[14] the point defects induced by irradiation were seen to introduce an additional term to the *ab* plane conductivity which was not of the flux-flow form. They analyzed their resistivity data using the form $\rho = (1/\rho_f + 1/\rho_P)^{-1}$ where ρ_f is the flux-flow resistivity and ρ_P the resistivity due to point defects. The latter had an activated form: $\rho_P = \rho_0 \exp\{-U(T,H)/T\}$, and the field dependence of the "plastic energy" was $U \sim H^{-0.7\pm0.1}$.

Let us consider the effect of uncorrelated disorder on the conductivity calculated from TDGL. We will model the point defects by adding a quenched random mass term to the free-energy functional

$$F_R[\Psi] = \int d^3\mathbf{r} \Big[\ldots + (\alpha + \alpha_R(\mathbf{r}))\,|\Psi|^2 + \ldots \Big], \tag{69}$$

where the random variables $\alpha_R(\mathbf{r})$ have zero average

$$\overline{\alpha_R(\mathbf{r})} = 0 \tag{70}$$

and δ-function correlations

$$\overline{\alpha_R(\mathbf{r})\ \alpha_R(\mathbf{r}')} = \frac{W_0}{2}\ \delta(\mathbf{r}-\mathbf{r}'). \tag{71}$$

The associated disordered TDGL can be written as

$$\Psi(\mathbf{r},t) = \int d\mathbf{r}' \int dt' G(\mathbf{r},t;\mathbf{r}',t') \left[\eta(\mathbf{r}',t') - \alpha_R(\mathbf{r}')\Psi(\mathbf{r}',t') - \beta|\Psi(\mathbf{r}',t')|^2\Psi(\mathbf{r}',t')\right] \tag{72}$$

or symbolically as

$$\Psi_1 = G_{1,2}\eta_2 - \alpha_{R2}G_{1,2}\Psi_2 - \beta G_{1,2}\Psi_2^*\Psi_2\Psi_2. \tag{73}$$

We have simply added the new term to eq. (15), hence $G_{1,2}$ remains the same, that is, the Green's function of the pure, linearized system.

Iterating this equation with $\beta = 0$ gives

$$\Psi_1 = G_{1,2}\eta_2 - \alpha_{R2}G_{1,2}G_{2,3}\eta_3 + \alpha_{R2}\alpha_{R3}G_{1,2}G_{2,3}G_{3,4}\eta_4 + O(\alpha_R^3). \tag{74}$$

Diagrammatically, we will represent α_R by a small square. There will be one arrow (Green's function) pointing into it and one out of it. The disorder averaging pairs up the α_R's, we represent this feature by a dashed line connecting the two squares. Because of the spatial δ function in the correlation of the disorder (71), squares connected by a dashed line represent the same point in space but different points in time. Thus as far as spatial integrals are concerned, diagrams in this perturbation expansion are identical to those found expanding the nonlinear term. It is the time integrals that make it different.

Figure 7 shows some diagrams that arise at the first order in an expansion in the disorder strength W_0. Note that if we were to draw the two points connected by the dashed line as one point, then we would end up with diagrams very much like those in Figure 2. (They would still differ by the number of circles.) In fact, the diagram in Fig. 7(d) gives zero contribution at $\mathbf{k} = \mathbf{0}$ for both σ_{xx} and σ_{zz} for the same reasons as that in Fig. 2(b). The diagram in Fig. 7(a) is Green's function renormalizing, those in (b) and (c) noise renormalizing, and that in (d) vertex-renormalizing.

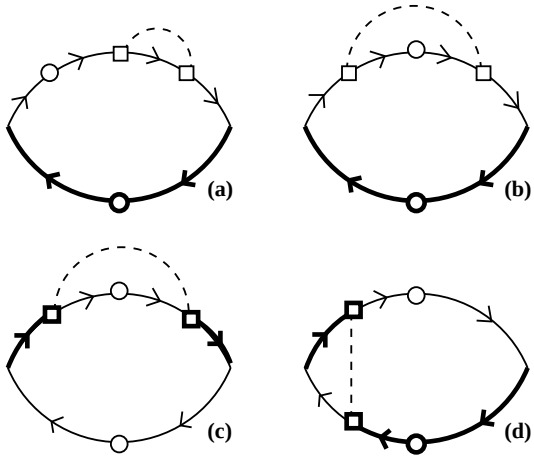

FIG. 7. Some diagrams at first-order in the disorder strength. Diagram 7(a) is Green's function renormalizing; diagrams 7(b) and (c) are noise renormalizing; and diagram 7(d) is vertex-renormalizing. The last is not only "down" but also zero at $\mathbf{k} = \mathbf{0}$.

Certain basic facts about the calculations do not change in the presence of disorder. For instance, in the calculation of $\sigma_{xx}(k_x, k_y = 0, k_z)$, it remains true that there is a maximum of two $n \geq 1$ Green's functions in diagrams contributing to the $\tilde{\alpha}/\hbar\omega_0 \to 0$ limit. Hence the diagram in Fig. 7(d) does not contribute to this order. Another invariant is that either the two $n \geq 1$ Green's functions meet each other at a noise average (as in Fig. 7(a) and (b)) or they each meet a vertex (as in Fig. 7(c)). The difference is now there are two types of vertices, the original quartic vertices and the new disorder induced vertices. From the case in which the $n \geq 1$ Green's functions meet at a noise average, one gets the disordered analog of the flux-flow formula with $\langle|\Psi_0|^2\rangle$ replaced by its disordered counterpart. (This particular subset of diagrams yields the $1/\rho_f$ in the Fendrich *et al.*[14] analysis.) From the case in which the two Green's functions meet quartic vertices, one gets the disordered analog of eq. (57).

Then there are new cases, like the noise-renormalizing diagram shown in Fig. 7(c). Evaluating it yields

$$\sigma_{xx}^{7(c)}(k_z) = \sigma_{xx}^{(G)}(\mathbf{0})\ \frac{(\pi-2)z_0}{2}\ \left[1 + \frac{1}{2}k_z^2\ell_c^2\right]^{-2}. \tag{75}$$

Note that we have factored out the pure Gaussian result; it multiplies a numerical factor and z_0, the dimensionless expansion parameter[33] for point disorder

$$z_0 = \frac{W_0}{16\pi\ell^2\xi_c\tilde{\alpha}^2}. \tag{76}$$

We have also included the diagram's k_z dependence. The c-axis length scale associated with this diagram, as well as those in Fig. 7 (a) and (b), is ℓ_c. As in the pure case, we can send the external momentum k_z through channel made entirely of $n = 1$ states. Recall that the points connected by the dashed line are the same point in space; consequently, in Fig. 7(c) the dashed line acts as a "short" allowing the external momentum k_z to pass through a channel comprised solely of $n \geq 1$ states.

By once again factoring out the higher Landau level Green's functions, this last calculation might be generalized to

$$\begin{aligned}\Sigma_{xx}^{(1)}(k_x, k_z) = \frac{e^{*2}W_0}{16k_BTm_{ab}^2}\int d(\mathbf{r}-\mathbf{r}')\int d(t-t')\int d\mathbf{r_5}\int dt_5\int dt_6\ \mathrm{e}^{ik_x(x-x')+ik_z(z-z')} \\ \Big(P_{1x}+P_{2x}^*\Big)\Big(P_{3x}+P_{4x}^*\Big)\Big\{G^*(\mathbf{r_2},t;\mathbf{r_5},t_5)G(\mathbf{r_3},t';\mathbf{r_5},t_6) \\ \langle\Psi_0(\mathbf{r_1},t)\Psi_0^*(\mathbf{r_5},t_5)\Psi_0(\mathbf{r_5},t_6)\Psi_0^*(\mathbf{r_4},t')\rangle_c + c.c.\Big\},\end{aligned} \tag{77}$$

where we imagine the remaining LLL object as being fully renormalized. The disorder average was performed with the result that the order parameter fields $\Psi_0(\mathbf{r_5}, t_5)$ and $\Psi_0^*(\mathbf{r_5}, t_5)$ are at the same point in space but different points in time. Note that the LLL object here is a four-point quantity and thus probes viscous effects even at $\mathbf{k} = \mathbf{0}$. The resummation suggested in eq. (77) is just one example of a new feature induced by the defects.

B. Correlated Disorder

We model columnar defects lying parallel to the c axis by changing the correlation of the disorder from a $3D$ delta function to a $2D$ delta function

$$\overline{a(\mathbf{r})\ a(\mathbf{r}')} = \frac{W_1}{2}\ \delta(x-x')\ \delta(y-y'). \tag{78}$$

For sake of comparison we calculated the diagram in Fig. 7(c) for columnar defects, obtaining

$$\sigma_{xx}^{7(c)}(k_z,0) = \sigma_{xx}^{(G)}(\mathbf{0})\ \frac{3z_1}{8}\ \left[\frac{8(-2+(1+k_z^2\xi_c^2/4)^{1/2}+(1+k_z^2\xi_c^2/4)}{3k_z^2\xi_c^2(1+k_z^2\xi_c^2/4)^2}\right], \tag{79}$$

where we have factored the result as above and z_1 is the dimensionless expansion parameter for columnar defects

$$z_1 = \frac{W_1}{16\pi\ell^2\tilde{\alpha}^2}. \tag{80}$$

Note that z_1 differs from z_0 by the absence of ξ_c in the denominator of z_1, making z_1 the larger of the two in the $\tilde{\alpha}\to 0$ limit. The c-axis length scale associated with the diagram in Fig. 7(c) is ξ_c. Points connected by a dashed line are no longer at the same point in space. They have different values of z; therefore, the dashed line no longer serves as a "short" for external momentum k_z and we can no longer send k_z through an exclusively $n\geq 1$ channel. The switch from the ℓ_c length scale for point defects to ξ_c for columnar defects in the evaluation of theses diagrams is in accord with the suggestion that correlated defects align pancake vortices enhancing their integrity.

We model planar defects by changing the disorder correlations to

$$\begin{aligned}\overline{a(\mathbf{r})\ a(\mathbf{r}')} &= \frac{W_{2x}}{2}\ \delta(x-x');\\ \overline{a(\mathbf{r})\ a(\mathbf{r}')} &= \frac{W_{2y}}{2}\ \delta(y-y'),\end{aligned} \tag{81}$$

where the former models planar defects parallel to the yz plane and the latter those parallel to the xz plane. When the electric field is in the x direction, the vortices move in the y direction. One might expect different results for vortices moving parallel to or perpendicular to the defects. Evaluation of the diagram in Fig. 7(c) is then

$$\begin{aligned}\sigma_{xx}^{7(c)}(k_z,0) &= \sigma_{xx}^{(G)}(\mathbf{0})\ \frac{3\sqrt{\pi}z_{2x}}{8\sqrt{2}}\ \left[\frac{8(-2+(1+k_z^2\xi_c^2/4)^{1/2}+(1+k_z^2\xi_c^2/4)}{3k_z^2\xi_c^2(1+k_z^2\xi_c^2/4)^2}\right];\\ \sigma_{xx}^{7(c)}(k_z,0) &= \sigma_{xx}^{(G)}(\mathbf{0})\ \frac{3\sqrt{\pi}z_{2y}}{8\sqrt{2}}\ \left[\frac{8(-2+(1+k_z^2\xi_c^2/4)^{1/2}+(1+k_z^2\xi_c^2/4)}{3k_z^2\xi_c^2(1+k_z^2\xi_c^2/4)^2}\right],\end{aligned} \tag{82}$$

where

$$z_{2i} = \frac{W_{2i}}{16\pi\ell\tilde{\alpha}^2} \tag{83}$$

(with $i=x$ or y) are the dimensionless expansion parameters for planar defects. For this particular diagram we find no difference between the xz and yz planar defects. The planar defect expansion parameter z_{2i} has the same $\tilde{\alpha}$ dependence and so the same temperature dependence as z_1. On the other hand, z_1 has an additional ℓ in the denominator so the magnetic field dependence of these expansion parameters is different.

VII. SUMMARY

We have investigated the conductivity in the vortex-liquid regime via perturbation theory. Using an approach in which an electric field is applied explicitly we showed that within the lowest Landau level (LLL) approximation the uniform ab plane conductivity, $\sigma_{xx}(\mathbf{0})$, is proportional to $\langle|\Psi_0|^2\rangle$ with a temperature-independent proportionality constant, to all orders in perturbation theory. This result elevates the derivation of the flux-flow formula to non-zero temperatures. We identified the subset of diagrams that yields the same result calculated within the Kubo formalism and conjectured that the remaining diagrams must cancel. We verified this cancellation to second order in

perturbation theory and also demonstrated that the cancellation does not extend to the nonlocal conductivity $\sigma_{xx}(\mathbf{k})$, allowing viscous effects to enter.

When it comes to the nonlocal conductivity and the issue of characteristic lengths, the present work has certainly raised more questions than it has answered. For instance, the lowest-order (Gaussian) diagram of the transverse ab-plane conductivity already revealed a long, temperature-dependent length; while all of the diagrams for the longitudinal ab-plane conductivity individually had short, temperature-independent length scales. If the longitudinal length scale is to grow long, as is suggested by its identification with shearing effects of a growing crystal, it will be through the combined effect of many diagrams. The nature of the diagrams that may lead to such an effect have been identified, but what remains unclear is whether the longitudinal and transverse length scales are independent or related.

There is a similar question regarding the c-axis. Every diagram contributing to the LLL approximation of σ_{zz} has ξ_c, the temperature-dependent correlation length, as its length scale. On the other hand, at each order in the perturbative expansion of σ_{xx}, the c-axis length scale is ℓ_c, a temperature-independent magnetic length. If $\sigma_{xx}(z-z')$ is to become substantially nonlocal as T is lowered, it will be through the combined effect of various orders. If the two length scales are long, it is unclear whether they will turn out to be essentially the same or distinct. In addition, there is the question of whether or not the ab-plane and c-axis length scales grow independently. Finally, these matters must be readdressed with regard to the nonlocal resistivity which may have its own distinct length scales.

We also examined the effect of disorder on the ab-plane conductivity. While there was a subset of diagrams that lead to the disordered analog of the flux-flow formula, there were other contributions that coupled to the viscous effects even at $\mathbf{k} = \mathbf{0}$. We also showed that diagrams contributing to the LLL approximation had as their c-axis length scale ℓ_c in the presence of point defects and ξ_c in the presence of columnar and planar defects.

Missing from this work is any consideration of what vector-potential fluctuations might do. Including them would require a new kind or vertex, one involving a Ψ, a Ψ^* and an $\mathcal{A}_\mu$, where $\mathcal{A}_\mu$ is the fluctuating part of the vector potential. The arguments leading to the flux-flow result may no longer hold when these new vertices are added. Also lacking are the effects of Maxwell's equations which are needed to form a complete set of equations. At low order these lead to back-flow effects and at higher orders may produce lattice effects. There are many challenging aspects of this problem to be resolved.

VIII. ACKNOWLEDGEMENTS

We would like to thank the authors of Ref.[5] for fruitful correspondence. We would also like to thank M.J.W. Dodgson, D.A. Huse, H. Jensen, A.J. McKane, N.K. Wilkin and J. Yeo for useful discussions. TB acknowledges the support of the Engineering and Physical Science Research Council under grant GR/K53208 and of the National Science Foundation under grant DMR9312476.

---

[1] H. Safar, P.L. Gammel, D.A. Huse, S.N. Majumdar, L.F. Schneemeyer, D.J. Bishop, D. López, G. Nieva and F. de la Cruz, Phys. Rev. Lett. **72**, 1272 (1994).
[2] C.D. Keener, M.L. Trawick, S.M. Ammirata, S.E. Hebboul and J.C. Garland, Phys. Rev B **55** R708 (1997).
[3] E.H. Brandt, Rep. Prog. Phys. **58**, 1465 (1995).
[4] Yu. Elstev and Ö. Rapp, Phys. Rev. Lett. **75**, 2446 (1995).
[5] D. López, E.F. Righi, G. Nieva and F. de la Cruz, Phys. Rev. Lett. **76**, 4034 (1996).
[6] M.C. Marchetti and D.R. Nelson, Phys. Rev. B **42**, 9938 (1990); Physica C **174** 40 (1991).
[7] D.A. Huse and S.N. Majumdar, Phys. Rev. Lett. **71**, 2473 (1993).
[8] C-Y. Mou, R. Wortis, A.T. Dorsey and D.A. Huse, Phys. Rev. B **51**, 6575 (1995).
[9] T. Blum and M.A. Moore, Phys. Rev. B **51**, 15359 (1995).
[10] R. Wortis and D.A. Huse, Phys. Rev. B **54**, 12413 (1996).
[11] S. Phillipson, M.A. Moore, T. Blum and T. Newman, in preparation.
[12] Y.B. Kim, C.F. Hempstead and A.R. Strnad, Phys. Rev. **139**, A1163 (1965).
[13] A. I. Larkin, Sov. Physics JETP **31**, 784 (1970).
[14] J.A. Fendrich, W.K. Kwok, J. Giapintzakis, C.J. van der Beek, V.M. Vinokur, S. Fleshler, U. Welp, H.K. Viswanathan and G.W. Crabtree, Phys. Rev. Lett. **74**, 1210 (1995).
[15] N. Wilkin and M. A. Moore Phys. Rev. B **50**, 10294 (1994).
[16] R. Ikeda, J. Phys. Soc. Jap. **64**, 1683 (1995); Z. Tesanovic and A.V. Andreev, Phys. Rev. B, **49**, 4064 (1994).

[17] G. Blatter, M.V. Feigel'man, V.B. Geshkenbein, A.I. Larkin and V.M. Vinokur, Rev. Mod. Phys. **66**, 1125 (1994).
[18] A. Schmid, Phys. Kondens. Materie **5**, 302 (1966); Phys. Rev. **180**, 527 (1969).
[19] L.P. Gor'kov and N.B. Kopnin, Sov. Phys. Usp. **18**, 496 (1976).
[20] A.T. Dorsey, Phys. Rev. B **46**, 8376 (1992).
[21] S. Ullah and A.T. Dorsey, Phys. Rev. B **44**, 262 (1991).
[22] R.S. Thompson and C.-R. Hu, Phys. Rev. Lett. **27**, 1352 (1971).
[23] G. Vecris and R.A. Pelcovits, Phys. Rev. B **44**, 2767 (1991).
[24] R.J. Troy and A.T. Dorsey, Phys. Rev. B, **47**, 2715 (1993).
[25] K.Maki, Prog. Theor. Phys. **39**, 897 (1968); R.S. Thompson, Phys. Rev. B **1** 327 (1970) ; V.V. Dorin, R.A. Klemm, A.A. Varlamov, A.I. Buzdin and D.V. Livanov, Phys. Rev. B **48**, 12951 (1993).
[26] R. Ikeda, T. Ohmi and T. Tsuneto, J. Phys. Soc. Jpn. **58**, 1377 (1989), *ibid.* **60**, 1051 (1991).
[27] G.J. Ruggeri and D.J. Thouless, J. Phys. F **6**, 2063 (1976).
[28] As happens in other cases, for instance with the specific heat, the exchange term gets "screened" and the Hartree approximation works better than Hartree-Fock at lower temperatures. See *e.g* R.F. Hassing, R.R. Hake and L.J. Barnes, Phys. Rev. Lett. **30**, 6 (1973).
[29] J. Yeo and M.A. Moore, Phys. Rev. Lett. **76**, 1142 (1996) and Phys. Rev. B **54**, 4218 (1996).
[30] M.A. Moore, Phys. Rev. B, **45**, 7336 (1992).
[31] M.J.W. Dodgson and M.A. Moore, Phys. Rev. B **55**, 3816 (1997).
[32] A.K. Kienappel, private communication.
[33] A. Fujita, S. Hikami and A.I. Larkin, Physica C **185-189**, 1883 (1991).